

Line Tension Reshapes Nucleation at Surface Edges: A Generalized Theory for Nanopore Activation

Yanchen Wu, Martin Z. Bazant, Allan S. Myerson, and Richard D. Braatz*
*Department of Chemical Engineering, Massachusetts Institute of Technology,
 77 Massachusetts Avenue, Cambridge, MA 02139, USA*
 (Dated: June 23, 2025)

Heterogeneous nucleation at surface edges is pervasive across nature and industry, yet the role of line tension, arising from asymmetric capillary interactions at geometric singularities, remains poorly understood. Herein we develop a generalized nucleation theory that explicitly incorporates line tension induced by edge pinning, thereby extending classical frameworks to account for nanoscale confinement and interfacial asymmetry. Through analytical treatment of droplet formation within geometrically defined nanopores, we derive a closed-form expression for the edge-pinned line tension as a function of Laplace pressure, pore geometry, and wettability. This formulation reveals that line tension can significantly reshape the nucleation energy landscape, introducing nontrivial dependencies on contact angle and pore morphology. Our results uncover a tunable, geometry-mediated mechanism for controlling nucleation barriers, offering predictive insight into phase transitions in confined environments and suggesting new strategies for design in applications ranging from nanofluidics to crystallization control.

Nucleation, the emergence of a new daughter phase from a metastable parent phase [1, 2], is fundamental to countless natural and technological processes, including cloud and ice formation [3–5], amyloid fibril aggregation in Alzheimer’s disease [6], pharmaceutical crystallization [7], and nanofabrication [8]. For over a century, classical nucleation theory (CNT) and its heterogeneous extension (hetCNT) have provided the foundational framework for describing nucleation in bulk and at idealized surfaces [9–14]. However, these models rely on oversimplified assumptions of smooth, regular geometries and neglect nanoscale features such as edges, crevices, and confinement, which are ubiquitous in real systems. In particular, the existence of line tension further complicates the problem and its role in wetting and nucleation remains poorly understood [15–19].

Despite extensive efforts to infer line tension values from contact angle measurements [20], particle detachment experiments [21], and nucleation rate analyses [22, 23], its magnitude and even sign remain controversial [24–27]. Line tension plays a significant role at the nanoscale, influencing wetting [28], nucleation [29, 30], boiling [31], and drying [32] in confined geometries. Nanopores, in particular, exhibit a variety of confinement-induced phenomena. For instance, vapor nucleation within nanopores governs biological gating and ion transport [33–35]. Capillary condensation, freezing transition, and intrusion-extrusion processes in confined pore geometries are strongly influenced by molecular layering [36], electrostatic interactions [37], network connectivity [38], and contact angle hysteresis [38], all of which can modulate nucleation pathways beyond classical expectations. The long-term stability of surface nanobubbles—central to hydrophobic interactions in biomolecular systems—has been linked to line tension and contact line pinning on nanoscale surface fea-

tures [39–42]. Nevertheless, existing models such as interface displacement model often introduce line tension as a phenomenological correction to classical models [17, 43, 44], decoupled from the actual geometry constrain of the substrate and contact line pinning, which may contribute to the long-standing ambiguity in its magnitude and sign.

Here we address this gap by developing a rigorous

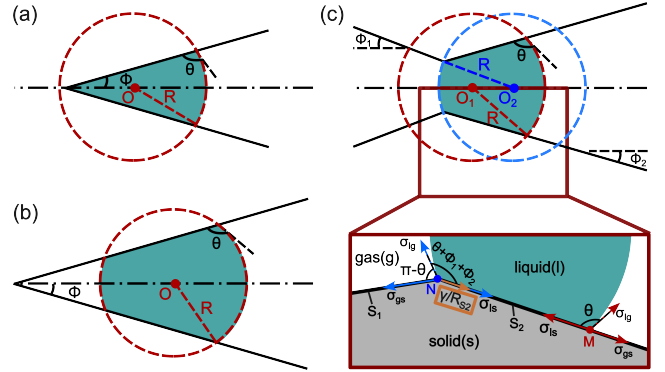


FIG. 1. Schematic cross-sectional view of critical nuclei (green, with radius R) forming within pore structures with given pore opening angles 2ϕ (or $2\phi_1$ and $2\phi_2$) and contact angles θ . (a) and (b) illustrate classical scenarios in smooth conical pores. (c) depicts a generalized asymmetric pore geometry, where a critical droplet bridges the neck between two sides with distinct opening angles (left: $2\phi_1$; right: $2\phi_2$). Red and blue dashed circles, centered at O_1 and O_2 , represent fitted curvature profiles on the right and left interfaces, respectively. The lower part of (c) zooms in on the three-phase contact region, showing a force balance sketch at the triple contact line. The points M and N denote the triple-phase contact locations, while S_1 and S_2 represent the inner pore surfaces. The surface edge at point N gives rise to a line tension γ , and R_{S2} is the curvature radius of the contact line at N projected on surface S_2 .

mathematical framework for heterogeneous nucleation that explicitly couples line tension to geometric confinement and contact line pinning. Unlike classical treatments that attribute line tension solely to molecular interactions, our approach isolates the geometric or pinning-induced contribution. We demonstrate that such contributions arise intrinsically from geometric confinement, independent of intermolecular forces, and can significantly alter nucleation behavior in nanoscale environments.

Focusing on droplet formation in pore structures with defined opening angles, we derive an analytic expression for the line tension in terms of the Laplace pressure, geometric parameters, and wettability. This formulation reveals that the pinning induced line tension is not an intrinsic material constant, but a geometry-dependent quantity that fundamentally modifies the nucleation barrier. Our results show how pore geometry and surface wettability can be tuned to control nucleation pathways, regulating nucleation energy barriers on demand. It opens a path toward rational design of nucleation processes, offering a bridge between fundamental interfacial physics and real-world control over phase transitions in confined systems.

To capture how line tension emerges and reshapes the nucleation process in pore structures, we consider a quasi-equilibrium liquid droplet nucleating inside a pore with geometrically defined edges, e.g., conical or asymmetric constrictions as seen in Fig. 1. The Gibbs free energy change related to the nucleation formation is

$$\Delta G = \Delta F_H - V \Delta p, \quad (1)$$

where ΔF_H is the variation in the Helmholtz free energy due to the formation of a cluster, which is formulated as

$$\Delta F_H = \sigma_{lg} A_{lg} + (\sigma_{ls} - \sigma_{gs}) A_{ls} + \gamma l, \quad (2)$$

where σ_{lg} , σ_{ls} , and σ_{gs} are interfacial tensions between liquid-gas, liquid-substrate, and gas-substrate, respectively. The parameters A_{lg} and A_{ls} denote liquid-gas and liquid-substrate interfacial areas, respectively. In the last term, γ is the line tension and l stands for the length of the triple contact line along the surface edge. Here, “line tension” is induced by an effective geometric energy correction ΔE_{geo} arising from the coupling between Laplace pressure and edge-induced confinement, rather than a molecular-scale quantity. We define $\gamma = \Delta E_{\text{geo}}/l$ to capture this scenario-dependent effect, offering insight into the long-standing ambiguity in its experimental determination.

The second term in the right-hand side of Eq. (1) is the volumetric free energy, in which Δp is the pressure difference between the droplet and the surrounding supersaturated vapor. Its value is closely related to the supersaturation S by

$$\Delta p = \frac{k_B T \ln S}{v_m}, \quad (3)$$

with k_B , T and v_m denoting the Boltzmann constant, temperature, and the molar volume, which are kept unchanged.

A nucleus will grow once the critical free energy barrier is overcome. The critical parameters for heterogeneous nucleation can be determined by minimizing the Gibbs free energy change. Thus, the critical nucleus corresponds to the condition $\partial \Delta G / \partial R = 0$, i.e.,

$$\left. \frac{\partial \Delta F_H}{\partial R} \right|_{R=R_c} - \Delta p \left. \frac{\partial V}{\partial R} \right|_{R=R_c} = 0 \quad (4)$$

where the critical nucleus radius R_c satisfies the Young-Laplace equation $\Delta p = 2\sigma_{lg}/R_c$. Throughout this work, we assume a constant liquid-gas surface tension σ_{lg} , so that the critical nucleus radius R_c depends solely on the pressure difference Δp or equivalently, on the supersaturation S . Under the further assumption of constant supersaturation, R_c is treated as a fixed value. The wetting behavior at the substrate is typically characterized by the Young contact angle θ , which is related to the interfacial tensions through Young’s equation $\cos \theta = (\sigma_{gs} - \sigma_{ls})/\sigma_{lg}$.

Fig. 1(a) and (b) illustrate classical scenarios of critical nucleus formation in smooth conical pores, in the absence of surface edge pinning effects. Specifically, panel (a) corresponds to the case where the pore is completely filled by the droplet, while panel (b) depicts a droplet forming as a spherical cap, intersecting only a portion of the pore interior. These classical configurations have been partially studied in previous works [14, 45], and a more detailed discussion is provided in the Supplemental Document. They serve as a baseline for comparison with the generalized model developed in this work.

In contrast to classical approaches that consider smooth conical pores and neglect the contact line contribution, we explicitly resolve its geometry and force balance at the three-phase junction on the surface edge for a more generalized pore geometry as shown in Fig. 1(c). In particular, we focus on pores with asymmetric opening angles, where sharp surface edges introduce geometric singularities that give rise to an additional capillary force that we interpret as line tension related force, accounting for the deviation of the apparent contact angle from the Young’s contact angle on the droplet covered inner pore surface (denoted as S_2 in Fig. 1(c)) near the edge N . We assume that the droplet shows an apparent contact angle of $\theta + \phi_1 + \phi_2$ on surface S_2 whereas it forms an apparent angle of θ on surface S_1 . At position M , far from the edge, Young’s equation applies and the local contact angle remains θ .

Through detailed geometrical analysis, we derive expressions for the droplet volume $V = V(\theta, \phi_1, \phi_2, R)$ and the interfacial areas A_{lg} and A_{ls} , as functions of the contact angle, geometric parameters, and droplet radius. By combining these expressions with Eq. (2) and Eq. (4), we

obtain a closed-form expression for a dimensionless line tension, defined as $\gamma^* =: \gamma/(\sigma_{lg}R_c)$. This expression serves as a predictive relation linking the critical radius of the nucleating droplet, the contact angle, and the local pore geometry (see Supplemental Document for the full derivation),

$$\gamma^* = \frac{\gamma}{\sigma_{lg}R_c} = -\frac{\cos(\theta + \phi_1)}{\sin \phi_2} [\cos(\theta + \phi_1 + \phi_2) - \cos \theta]. \quad (5)$$

This equation shares the same form as the classical modified Young's equation considering the line tension effect. The physical interpretation is that the line-tension-induced capillary force accounts for the deviation of the apparent contact angle $\theta + \phi_1 + \phi_2$ on surface S_2 from the intrinsic Young's angle θ . The prefactor $-\frac{R_c \cos(\theta + \phi_1)}{\sin \phi_2}$ corresponds exactly to the radius of curvature of the contact line at N projected onto surface S_2 , denoted as R_{s2} in Fig. 1(c). The above geometric and force balance analysis reveals that this type of line tension emerges as a mechanical consequence of Laplace pressure under geometric confinement and pinning effects.

This insight, in turn, validates the inclusion of the line contribution in Eq. (2). It is noteworthy, however, that the length l in Eq. (2) specifically refers only to the contact line along the surface edge. Possible contributions from the contact line on smooth surfaces, where line tension can arise from intermolecular or long-range forces [46], have been neglected.

Building upon this theoretical framework of edge-pinned line tension, we introduce a geometric parameter $f(\theta, \phi_1, \phi_2)$ to characterize the ratio of the critical energy barrier in heterogeneous nucleation to that of the homogeneous nucleation, i.e.,

$$f(\theta, \phi_1, \phi_2) = \frac{\Delta G_c}{\Delta G_{\text{hom},c}} = \sum_{i=1}^3 f_i(\theta, \phi_1, \phi_2), \quad (6)$$

where $\Delta G_{\text{hom},c}$ and f_i are

$$\begin{aligned} \Delta G_{\text{hom},c} &= \frac{4}{3} \pi R_c^2 \sigma, \\ f_1 &= \frac{3 \cos^2 \theta_1}{2 \sin \phi_2} [\cos(\theta + \phi_1 + \phi_2) - \cos \theta], \\ f_2 &= \frac{3}{4} \left[4 - 2 \sin \theta_1 - 2 \sin \theta_2 - \frac{\cos \theta}{\sin \phi_2} (\cos^2 \theta_2 - \cos^2 \theta_1) \right], \\ f_3 &= -\frac{1}{2} \left[\sum_{i=1}^2 (2 + \sin \theta_i)(1 - \sin \theta_i)^2 + \frac{\cos^3 \theta_2 - \cos^3 \theta_1}{\tan \phi_2} \right], \end{aligned}$$

where $\theta_i := \pi - \theta - \phi_i$ ($i = 1, 2$). The geometric parameters f_1 , f_2 , and f_3 are contributions from the contact line, surface and bulk energy terms, respectively. The factor f retains explicit dependence on contact angle θ and pore geometry (ϕ_1, ϕ_2) , allowing us to assess quantitative influence of these factors to the nucleation behavior.

Remarkably, we find the line tension effect significantly alters nucleation, with the energy barrier highly tunable via pore asymmetry and wettability. Fig. 2(a) illustrates the geometric parameter f as a function of the contact angle for different opening angles of the pore. We first plot the predictions from the classical nucleation theory for critical droplets in conical pores with different opening angles, as indicated by dot dashed lines. For comparison, we also present predictions from our model incorporating line tension effects at the surface edge (referred to as the LT model), shown as solid lines. In this case, we consider asymmetric pores with a fixed left opening angle $2\phi_1 = 0$ and varying right opening angles $2\phi_2$. Additional results for $\phi_1 = -20^\circ, 60^\circ$, and 90° are provided in the Supplemental Document. Our LT model predicts a pronounced suppression of the nucleation barrier compared to the classical model, especially at moderate wettability, namely, from $\theta = 90^\circ$ to $\theta = \theta_i$, where θ_i denotes the intersection point between the solid and dot dashed lines. The shaded region quantifies the suppression of nucleation attributable to line tension effect, which classical theory neglects. In contrast, under strongly hydrophobic conditions with $\theta > \theta_i$, the nucleation barrier in asymmetric pores exceeds that of conical pores. The Inset schematically illustrate a nucleated droplet within an asymmetric pore geometry characterized by $\phi_1 = 0$ and an adjustable ϕ_2 .

Fig. 2(b) shows the geometric factor f_1 (solid lines) and the dimensionless line tension factor γ^* (dot dashed lines) as functions of the contact angle, both predicted by the LT model. It indicates that surface-edge pinning becomes profound at moderate contact angles within the range $\theta \in (90^\circ, \theta_c)$, where the threshold angle $\theta_c = 180^\circ - 0.5\phi_2$. Within this regime, the line tension contributes a net negative energy. A striking finding is the non-monotonic behavior of the line tension factor and the associated geometric factor f_1 with contact angle. Local minima in f_1 are observed within $\theta \in (90^\circ, \theta_c)$ and these minima correspond to the largest deviations between LT models and the classical models.

Fig. 2(c) shows that the sum of geometric parameters from the volume and surface energy contribution $f_2 + f_3$ monotonically increases with contact angle. Since the contribution from line tension is relatively smaller, f still monotonically increases with contact angle, but the increase rate is different from that of $f_2 + f_3$. It should be noted that, the contact angle range $\theta \in (90^\circ, \theta_c)$ is divided into two intervals, i.e. I) $\theta \in (90^\circ, \theta_i)$ and II) $\theta \in (\theta_i, \theta_c)$. In the first interval (shaded areas in Fig. 2(a)), the negative line energy leads to the lower nucleation barrier for asymmetric pores, while in the second interval, the pinning effect changes the droplet profile, leading to the increase of the sum $f_2 + f_3$, which dominant over the line tension effect, so that the nucleation barrier for asymmetric pores becomes higher than that of the conical pores.

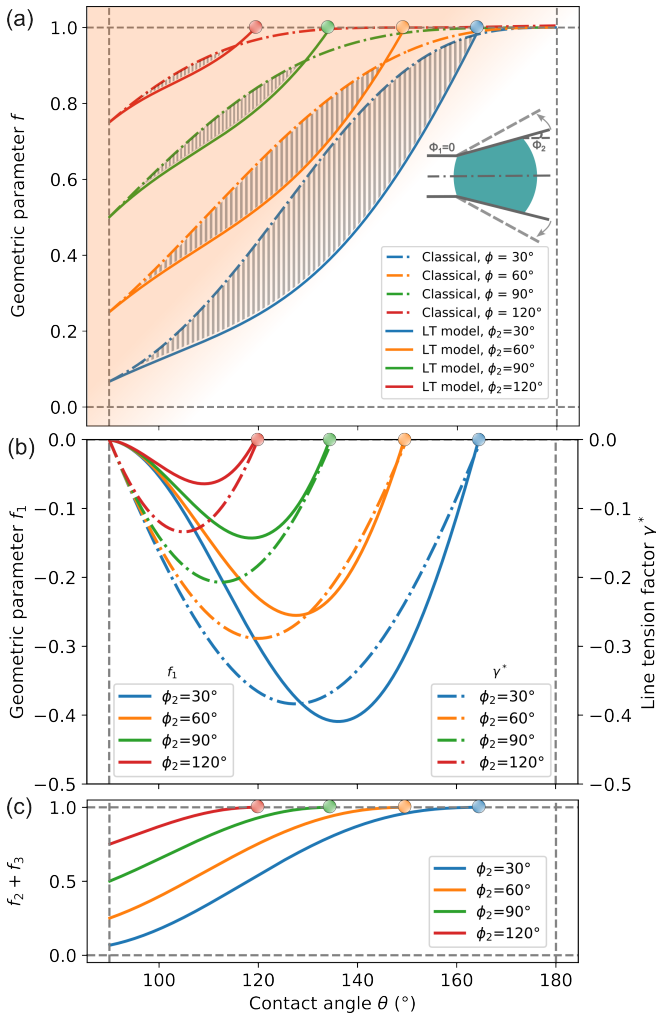


FIG. 2. Geometrical parameters of critical nuclei as a function of contact angles θ for a fixed left opening angle $2\phi_1 = 0$ and varying right opening angles $2\phi_2$. (a) Comparison between predictions from the line-tension (LT) model and classical models for droplets in conical pores without pinning. Shaded regions indicate deviations arising from the inclusion of line tension. The inset illustrates the pore geometry and the nucleated droplet configuration. (b) and (c) show the variations of geometrical parameters from line energy and surface energy contributions, respectively, with respect to θ . Panel (b) also includes the corresponding dimensionless line tension γ^* as a reference. Colored dots in (a)–(c) highlight the conditions where homogeneous nucleation occurs, representing the upper limit of θ for which the LT model remains valid.

When $\theta = \theta_c$, the droplet becomes suspended, symmetrically positioned between S_1 and S_2 , and the pinning effect vanishes. In this configuration, the spherical droplet exhibits identical contact angles with both the left and right pore walls (or S_1 and S_2). This geometrically induced upper limit for the contact angle ($\theta_c = 180^\circ - 0.5\phi_2$) represents a critical threshold for heterogeneous nucleation, as indicated by the colored circles in Fig. 2(a)–(c). This limit is absent in classical

frameworks for conical pores and establishes a fundamental constraint on nucleation or phase transition in nanoconfinement. This state corresponds to the critical case where the droplet becomes spherical and achieves a homogeneous nucleation state with $f = 1$. The upper limit contact angle $\theta_c = 180^\circ - 0.5\phi_2$ aligns with our previous theoretical prediction for capillary adsorption of droplets into a funnel-like structure confirmed by phase-field simulations [47]. For even more hydrophobic scenarios with $\theta > \theta_c$, the droplet maintains a spherical shape, effectively detaching from the right wall of the pore. In such cases, the nucleation barrier becomes identical to that of homogeneous nucleation, again characterized by $f = 1$.

As the right opening angle $2\phi_2$ decreases, the line tension contribution becomes more profound, facilitating nucleation over a broader range of contact angles. This trend is evident from the enlarged shaded regions in Fig. 2(a) as ϕ_2 decreases from 120° to 30° . Specifically, when $\phi_2 > 120^\circ$ (i.e., the pore takes on a thorn-like geometry), the shaded area is expected to largely decrease due to the reduced contribution of line energy and the lowering of θ_c . In this case, the critical nucleus droplet shows a spherical shape over a wider range of contact angles ($\theta > \theta_c = 180^\circ - 0.5\phi_2$), consistent with the classical Cassie-Baxter model. This model predicts that nano-/microstructures can induce superhydrophobicity by minimizing droplet–substrate contact, even at low intrinsic contact angles [48].

To further explore the effect of pore asymmetry, we fix ϕ_2 and vary ϕ_1 to examine a broader range of pore geometries. Fig. 3(a)–(c) illustrate how the geometric parameter f and the line tension factor γ^* evolve with θ for increasing ϕ_1 under fixed values of $\phi_2 = 30^\circ, 60^\circ, 90^\circ$, respectively. The valid contact angle range for the LT model is defined as $(\theta_0, \theta_c]$, where $\theta_0 = \max\{90^\circ - \phi_1, 90^\circ - \phi_2\}$ (see Supplemental Document for an explanation). As presented in Fig. 3(a), when $\phi_1 = -30^\circ$, the pore shows a conical geometry, thus the LT model prediction aligns with that of the classical model with $\phi = 30^\circ$ particularly in the highly hydrophobic regime. This agreement arises because the LT model assumes equal curvature radii on both sides of the droplet. In this special case, the LT model recovers the classical solution corresponding to the case shown in Fig. 1(b), rather than (a). As ϕ_1 increases to $\phi_1 = -10^\circ$ and 10° , the geometric factor f continues to increase with θ , though at different rates depending on the specific left-side angle $2\phi_1$. A further increase to $\phi_1 = 30^\circ$ and 50° introduces a non-monotonic trend in the f – θ relationship, attributed to the enhanced influence of line tension. The occurrence of negative values of f in certain θ ranges reflects the dominance of line tension in driving nucleation under those geometric configurations.

Similar to the previous discussion in Fig. 2, there is an upper limit contact angle $\theta_c = 180^\circ - 0.5(\phi_1 + \phi_2)$ for the LT model which corresponds to the critical case where the

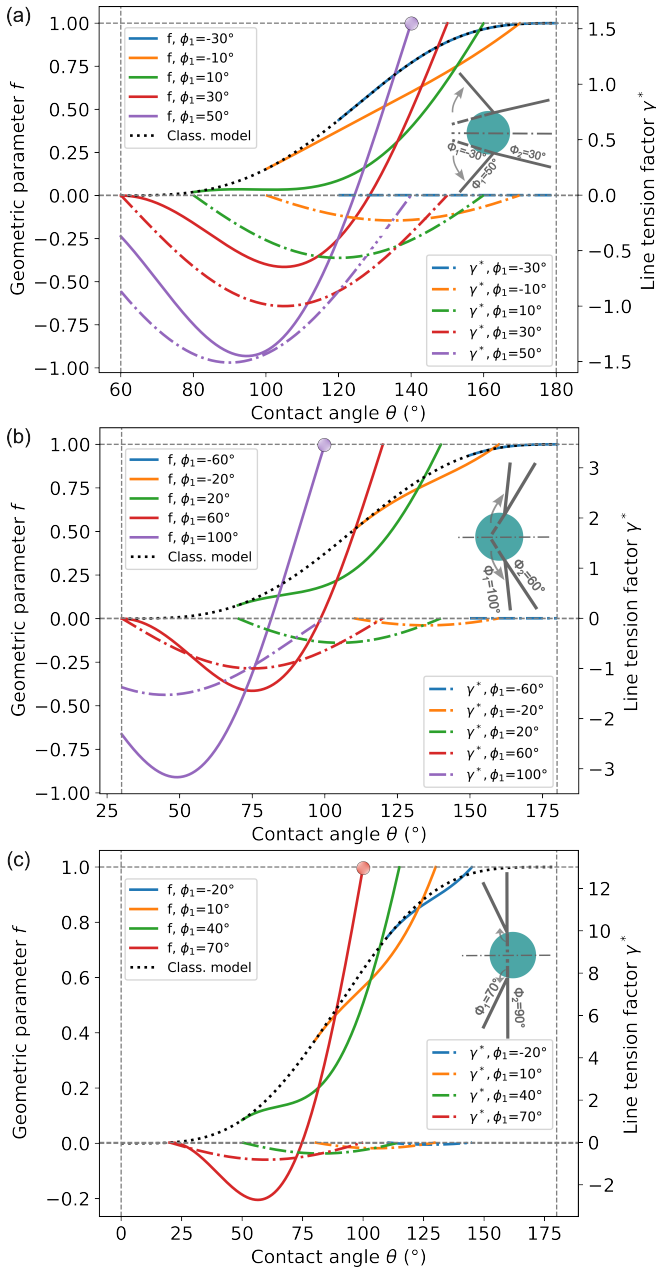


FIG. 3. Geometrical parameters and line tension factors of critical nuclei as functions of the contact angle θ for fixed ϕ_2 and varying ϕ_1 . The insets depict the critical nucleus configurations within the pore structures, matching the colored dots. Panels (a)–(c) represent cases with $\phi_2 = 30^\circ, 60^\circ, 90^\circ$, respectively. Predictions from classical models for droplets in smooth conical pores with $\phi = \phi_2$ are indicated as dotted lines for comparison.

droplet transitions into a homogeneous nucleation state with $f = 1$ and $f_1 = 0$. This critical state is indicated by the violet circle in Fig. 3(a) for $\phi_1 = 50^\circ$, and by the violet and red circles in Fig. 3(b,c) for $\phi_1 = 100^\circ$ and 70° , respectively, with corresponding schematic insets. It is also found that both θ_i and θ_c decrease with increasing

ϕ_1 . Similar to Fig. 2, the whole contact angle range is divided into two regimes: I) a lower-barrier regime for $\theta < \theta_i$, where line tension reduces the nucleation barrier; II) a higher-barrier regime for $\theta > \theta_i$, where the nucleation barrier increases relative to classical predictions. Both asymmetric and conical pores can reframe nucleation relative to the homogeneous case, reaffirming that homogeneous nucleation represents the upper limit of the nucleation barrier [49]. Fig. 3(b) and (c) present analogous trends for larger right-side angles $\phi_2 = 60^\circ$ and 90° , respectively. However, the tunable range of contact angles changes as ϕ_2 varies and the influence of line tension significantly changes compared to the case with a smaller half-opening angle ($\phi_2 = 30^\circ$). Overall, the LT model enables the construction of a comprehensive energy landscape for nucleation in diverse pore geometries, including asymmetric cases, conical shapes, stepped edges, and crevices, highlighting the model's broad applicability to realistic nano-/microstructured systems.

The above detailed investigation reveals one nontrivial feature. For a given pore geometry, the line tension term becomes especially significant when a particular contact angle is achieved. For example, with $\phi_1 = 0^\circ$ and $\phi_2 = 30^\circ$ (see Fig. 2), the line tension factor reaches a minimum $\gamma_{\min}^* \approx -0.4$ at $\theta = 125^\circ$. Assuming a critical radius of water nucleus $R_c = 50$ nm [50] and a surface tension $\sigma_{lg} = 0.07$ N/m, Eq. (5) yields a line tension of approximately -1.4×10^{-9} N—an order of magnitude larger than previously reported values of 10^{-11} to 10^{-10} N for water droplets on the flat quartz considering intermolecular forces [51]. By tuning R_c , pore geometry, and wettability, the line tension can even span several orders of magnitude, helping to explain the wide variability seen in the literature [52]. This may also explain the large deviations from classical predictions observed in nanoscale systems such as the anomalous stability of nanobubbles in cylindrical pores [32] or on surfaces under pinning [53], pore size and shape dependence of nucleation rate [50, 54–56], shifts in ice nucleation due to nanoscale texture [57], and wettability-dependent evaporation rates in nanopores [58].

To conclude, we extend classical nucleation theory to explicitly incorporate line tension arising from surface-edge pinning, uncovering a confinement-dominated regime of nucleation. Unlike classical line-tension models for smooth surfaces that often assume an ill-defined molecular-scale force, our approach treats line tension as a mechanical consequence of curvature and Laplace pressure for droplets confined near surface edges. It not only provides a quantitative expression for the edge-pinned line tension in confined systems, but also exposes how geometry and wetting jointly govern nucleation thresholds. These insights extend far beyond idealized nucleation models and offer a physically grounded tool for understanding and controlling nucleation in confined systems with broad applications in areas such as targeted drug de-

livery, pharmaceutical crystallization, and nanofabrication. The geometry-tailored line tension effect may provide a route to control nucleation at will, replacing trial-and-error design with predictive strategies. While direct experimental validation is beyond this work's scope, the proposed model is testable via precision experiments on tailored pore geometries. Looking forward, this framework can be generalized to incorporate fluctuations [59], instabilities [60], active wetting [61], and even two-step nucleation [62], laying the foundation for a unified theory of phase transitions [63] and nanobubbles [40] under nano-scale confinement, where geometrical edge effects are essential.

This research was supported by the U.S. Food and Drug Administration under the FDA BAA-22-00123 program, Award Number 75F40122C00200.

* braatz@mit.edu

- [1] J. W. Gibbs, *American Journal of Science* **3**, 441 (1878).
- [2] P. G. Debenedetti, Y.-Y. Kim, F. C. Meldrum, and H. Tanaka, *The Journal of Chemical Physics* **160** (2024).
- [3] U. Dusek, G. Frank, L. Hildebrandt, J. Curtius, J. Schneider, S. Walter, D. Chand, F. Drewnick, S. Hings, D. Jung, *et al.*, *Science* **312**, 1375 (2006).
- [4] T. W. Wilson, L. A. Ladino, P. A. Alpert, M. N. Breckels, I. M. Brooks, J. Browse, S. M. Burrows, K. S. Carslaw, J. A. Huffman, C. Judd, *et al.*, *Nature* **525**, 234 (2015).
- [5] J. M. Campbell and H. K. Christenson, *Physical Review Letters* **120**, 165701 (2018).
- [6] J. Sevigny, P. Chiao, T. Bussière, P. H. Weinreb, L. Williams, M. Maier, R. Dunstan, S. Salloway, T. Chen, Y. Ling, *et al.*, *Nature* **537**, 50 (2016).
- [7] S. M. Guthrie, D.-M. Smilgies, and G. Giri, *Crystal Growth & Design* **18**, 602 (2018).
- [8] K.-J. Wu, C. Edmund, C. Shang, and Z. Guo, *Progress in Materials Science* **123**, 100821 (2022).
- [9] R. O. Piuco, C. J. Hermes, C. Melo, and J. R. Barbosa Jr, *Experimental Thermal and Fluid Science* **32**, 1710 (2008).
- [10] N. H. Fletcher, *The Journal of Chemical Physics* **29**, 572 (1958).
- [11] L. R. Gómez, N. A. García, V. Vitelli, J. Lorenzana, and D. A. Vega, *Nature Communications* **6**, 6856 (2015).
- [12] R. Narhe and D. Beysens, *Physical Review Letters* **93**, 076103 (2004).
- [13] A. Cacciuto, S. Auer, and D. Frenkel, *Nature* **428**, 404 (2004).
- [14] S. K. Singha, P. K. Das, and B. Maiti, *The Journal of Chemical Physics* **143**, 204703 (2015).
- [15] R. Gretz, *Surface Science* **5**, 239 (1966).
- [16] G. Navascués and P. Tarazona, *Journal of Chemical Physics* **75**, 2441 (1981).
- [17] A. Amirfazli and A. Neumann, *Advances in Colloid and Interface Science* **110**, 121 (2004).
- [18] L. Schimmele, M. Napiórkowski, and S. Dietrich, *The Journal of Chemical Physics* **127** (2007).
- [19] F. Wang, H. Zhang, and B. Nestler, *Physical Review Letters* **133**, 246201 (2024).
- [20] J. K. Berg, C. M. Weber, and H. Riegler, *Physical Review Letters* **105**, 076103 (2010).
- [21] T. Kolarov, A. Scheludko, and D. Exerowa, *Transactions of the Faraday Society* **64**, 2864 (1968).
- [22] B. Toshev, D. Platikanov, and A. Scheludko, *Langmuir* **4**, 489 (1988).
- [23] A. I. Hienola, P. Winkler, P. Wagner, H. Vehkamäki, A. Lauri, I. Napari, and M. Kulmala, *The Journal of Chemical Physics* **126** (2007).
- [24] B. M. Law, *Physical Review Letters* **72**, 1698 (1994).
- [25] B. H. Tan and H. An, *Physical Review Letters* **134**, 074001 (2025).
- [26] J. Möller, A. Schottelius, M. Caresana, U. Boesenberg, C. Kim, F. Dallari, T. A. Ezquerro, J. M. Fernández, L. Gelisio, A. Glaesener, *et al.*, *Physical Review Letters* **132**, 206102 (2024).
- [27] M. Buchanan, *Nature Physics* **20**, 1038 (2024).
- [28] V. Raspal, K. Awitor, C. Massard, E. Feschet-Chassot, R. Bokalawela, and M. Johnson, *Langmuir* **28**, 11064 (2012).
- [29] S. Auer and D. Frenkel, *Physical Review Letters* **91**, 015703 (2003).
- [30] A. Tinti, A. Giacomello, Y. Grosu, and C. M. Casciola, *Proceedings of the National Academy of Sciences* **114**, E10266 (2017).
- [31] A. Giacomello, *The Journal of Chemical Physics* **159** (2023).
- [32] L. Guillemot, T. Biben, A. Galarneau, G. Vigier, and É. Charlaix, *Proceedings of the National Academy of Sciences* **109**, 19557 (2012).
- [33] O. Beckstein and M. S. Sansom, *Proceedings of the National Academy of Sciences* **100**, 7063 (2003).
- [34] J. H. Walther, K. Ritos, E. R. Cruz-Chu, C. M. Megaridis, and P. Koumoutsakos, *Nano Letters* **13**, 1910 (2013).
- [35] G. Paulo, K. Sun, G. Di Muccio, A. Gubbiotti, B. Morozzo della Rocca, J. Geng, G. Maglia, M. Chinappi, and A. Giacomello, *Nature Communications* **14**, 8390 (2023).
- [36] M. Z. Bazant and Z. P. Bazant, *Journal of the Mechanics and Physics of Solids* **60**, 1660 (2012).
- [37] T. Zhou, M. Mirzadeh, R. J.-M. Pellenq, and M. Z. Bazant, *Physical Review Fluids* **5**, 124201 (2020).
- [38] M. B. Pinson, T. Zhou, H. M. Jennings, and M. Z. Bazant, *Journal of Colloid and Interface Science* **532**, 118 (2018).
- [39] Y. Liu and X. Zhang, *The Journal of chemical physics* **138** (2013).
- [40] D. Lohse and X. Zhang, *Reviews of Modern Physics* **87**, 981 (2015).
- [41] Y. Sun, G. Xie, Y. Peng, W. Xia, and J. Sha, *Colloids and Surfaces A: Physicochemical and Engineering Aspects* **495**, 176 (2016).
- [42] B. H. Tan, H. An, and C.-D. Ohl, *Current Opinion in Colloid & Interface Science* **53**, 101428 (2021).
- [43] J. Indekeu, *Physica A: Statistical Mechanics and its Applications* **183**, 439 (1992).
- [44] C. Bauer and S. Dietrich, *The European Physical Journal B-Condensed Matter and Complex Systems* **10**, 767 (1999).
- [45] G. R. Willmott, C. Neto, and S. C. Hendy, *Soft Matter* **7**, 2357 (2011).
- [46] J. Joanny and P. De Gennes, *Journal of Colloid and Interface Science* **111**, 94 (1986).

- [47] Y. Wu, F. Wang, W. Huang, M. Selzer, and B. Nestler, *Physical Review Fluids* **7**, 054004 (2022).
- [48] F. Wang, Y. Wu, and B. Nestler, *Advanced Materials* **35**, 2210745 (2023).
- [49] X. Liu, *The Journal of Chemical Physics* **112**, 9949 (2000).
- [50] R. P. Sear, *Journal of Physics: Condensed Matter* **19**, 033101 (2007).
- [51] T. Pompe and S. Herminghaus, *Physical Review Letters* **85**, 1930 (2000).
- [52] G. Whyman, E. Bormashenko, and T. Stein, *Chemical Physics Letters* **450**, 355 (2008).
- [53] B. H. Tan, H. An, and C.-D. Ohl, *Physical Review Letters* **120**, 164502 (2018).
- [54] N. E. Chayen, E. Saridakis, and R. P. Sear, *Proceedings of the National Academy of Sciences* **103**, 597 (2006).
- [55] A. J. Page and R. P. Sear, *Physical Review Letters* **97**, 065701 (2006).
- [56] Y. Diao, T. Harada, A. S. Myerson, T. Alan Hatton, and B. L. Trout, *Nature Materials* **10**, 867 (2011).
- [57] C. Gurganus, J. Charnawskas, A. Kostinski, and R. Shaw, *Physical Review Letters* **113**, 235701 (2014).
- [58] J. Fan, H. Wu, and F. Wang, *Physics of Fluids* **32** (2020).
- [59] M. Fitzner, G. C. Sosso, F. Pietrucci, S. Pipolo, and A. Michaelides, *Nature Communications* **8**, 2257 (2017).
- [60] E. Theisen, M. Vogel, C. Lopez, A. Hirska, and P. Steen, *Journal of Fluid Mechanics* **580**, 495 (2007).
- [61] S. Liese, X. Zhao, C. A. Weber, and F. Jüllicher, *Proceedings of the National Academy of Sciences* **122**, e2403083122 (2025).
- [62] D. Erdemir, A. Y. Lee, and A. S. Myerson, *Accounts of Chemical Research* **42**, 621 (2009).
- [63] A. Davoodabadi and H. Ghasemi, *Advances in Colloid and Interface Science* **290**, 102385 (2021).